

# Landslides Triggered by the 2020 Qiaojia $M_w$ 5.1 Earthquake, Yunnan, China: Distribution, Influence Factors and Tectonic Significance

Xiangli He<sup>1,2</sup>, Chong Xu<sup>1,2</sup>, Wenwen Qi<sup>1,2</sup>, Yuandong Huang<sup>3</sup>, Jia Cheng<sup>1</sup>, Xiwei Xu<sup>1</sup>, Qi Yao<sup>4</sup>, Yongkun Lu<sup>5</sup>, Boyang Dai<sup>5</sup>



1. National Institute of Natural Hazards, Ministry of Emergency Management of China, Beijing 100085, China

2. Key Laboratory of Compound and Chained Natural Hazards Dynamics (Under Construction), Ministry of Emergency Management of China, Beijing 100085, China

3. China University of Geosciences, Beijing 100083, China

4. China Earthquake Networks Center, Beijing 100045, China

5. Yunnan Earthquake Agency, Kunming 650224, China

 Xiangli He: <https://orcid.org/0000-0002-2863-4457>;  Chong Xu: <https://orcid.org/0000-0002-3956-4925>

**ABSTRACT:** On May 18, 2020, an  $M_w$ 5.1 earthquake occurred in Qiaojia County, Yunnan Province, China. This moderate-sized event triggered massive coseismic landslides, resulting in some damage. In this work, through visual interpretation of high-resolution (0.8–2 m) Gaofen satellite images before and after the earthquake, 167 landslides were delineated, 18 of which were inspected in the field. Using the landslide number density (LND) and landslide area percentage (LAP), we characterized the spatial distribution of these landslides, and analyzed their possible influence factors and tectonic significance. The results show that these landslides are distributed mostly in the NW-SE direction, roughly parallel to the long axis of seismic intensity zones and the strike of the Xiaohe-Baogunao fault (XBF). The LND and LAP decrease with increasing distances to the fault and from the epicenter to fault ends of the XBF. These permit to suggest that the seismogenic fault of the Qiaojia earthquake is likely a hidden branch of the XBF. All of the landslides induced by this event occurred in the region with the seismic intensity of six degrees or greater of the 2014  $M_w$ 6.2 Ludian earthquake. Therefore, it was inferred that the 2020 Qiaojia earthquake was probably the subsequent release of accumulated elastic strain after the 2014 Ludian earthquake in a same tectonic stress regime.

**KEY WORDS:** Qiaojia earthquake, landslide inventory, spatial distribution, seismogenic fault, Ludian earthquake.

## 0 INTRODUCTION

Many studies have been conducted on the mechanism, spatial distribution pattern, and risk assessment of earthquake-triggered landslides (Xu and Xu, 2021; Fan et al., 2019; Xu C et al., 2014a; Dai et al., 2011; Khattak et al., 2010). In such research, an integrated coseismic landslide database is very important (Xu C, 2015a; Xu C et al., 2014a; Harp et al., 2011; Keefer, 2002). Wicczorek (1984) pointed out that a detailed landslide map can provide information to engineering geologists for assessing landslide hazard. Chen S et al. (2020) suggested that a coseismic landslide inventory can be used to determine the susceptibility of slopes to landsliding after earthquakes and provide a valid reference for emergency rescue. Based on field investigations, advanced technologies of remote sensing and

commonly accepted landslide-mapping principles, many detailed earthquake-induced landslide inventories have been established for seismic events in recent decades, such as the 1927  $M$ 8.0 Gulang, China (Xu et al., 2020), 1999  $M_w$ 7.7 Chi-Chi, Taiwan, China (Liao and Lee, 2000), 2008  $M_w$ 7.9 Wenchuan, China (Xu C et al., 2014a; Parker et al., 2011), 2015  $M_w$ 7.8 Gorkha, Nepal (Kargel et al., 2016; Xu et al., 2016), and the 2017  $M_w$ 6.5 Jiuzhaigou, China earthquakes (Tian et al., 2019). So far, most of work on this issue focuses on major events, while moderate-sized earthquakes sometimes can also induce significant slope failure and relevant studies remain rare. On May 18, 2020, an  $M_w$ 5.1 quake happened in Qiaojia County, Yunnan, China (hereafter called the Qiaojia earthquake). Unexpectedly, this earthquake is more destructive than other earthquakes with same magnitude, triggering massive landslides. Therefore, it is also necessary to investigate the coseismic landslides of such moderate-sized earthquakes.

In principle, a complete inventory not only records spatial locations of landslides, but also contains the influencing factors of landslide occurrence. A comprehensive coseismic landslide inventory is an important part of earthquake hazard assessment (Xu C, 2015a; Guzzetti et al., 2012; Harp et al., 2011). Xu C et

\*Corresponding author: [xc1111111@126.com](mailto:xc1111111@126.com)

© China University of Geosciences (Wuhan) and Springer-Verlag GmbH Germany, Part of Springer Nature 2021

Manuscript received March 9, 2021.

Manuscript accepted June 3, 2021.

al. (2014a) used both the landslide area percentage (LAP) and the landslide number density (LND) to correlate landslides triggered by the 2008 Wenchuan  $M_w$ 7.9 earthquake with geological, topographical and seismic conditions. Cui et al. (2021) linked the landslides triggered by 2018  $M_w$ 6.6 Hokkaido earthquake to nine influencing factors to implement a hazard assessment of coseismic landslides, which contributes to landslide hazard prevention and reduction and reconstruction of the affected area. Vanani et al. (2021) selected some controlling factors to revise the landslides inventory of the 1990 Rudbar-Manjil ( $M_w$ 7.3) earthquake and identified the areas prone to landsliding, using a multimodal distribution including LND, LAP, landslide area and landslide volume. In general, the influence factors of landslides can be classified into three categories: geology, topography and seismology. Besides, in view of the close relationship between coseismic landslide distribution, seismogenic structure, and seismic intensity, it is possible to help recognize the seismogenic fault and seismic rupture properties using information from landslide inventories

(Shao et al., 2019; Wu et al., 2018; Xu, 2015b; Xu and Xu, 2014).

The epicenter of the 2020 Qiaojia earthquake is only about 20 km away from that of the 2014  $M_w$ 6.2 Ludian earthquake. Both are located on the border between the South China Block and the eastern margin of the Tibetan Plateau (Fig. 1). The calculation of Coulomb stress suggested that the Ludian earthquake has influenced the stress state of adjacent active fault systems, and might have triggered subsequent aftershocks (Miao and Zhu, 2016; Xu X W et al., 2014). While whether the 2020 Qiaojia event was associated with such impact remains unclear.

In this work, based on field surveys and satellite image interpretation, a landslide inventory for the Qiaojia earthquake was prepared. Then using two parameters, LND and LAP, the spatial distribution of these landslides was characterized. In addition, its correlation with ten factors, involving topography, geology and seismology, was analyzed. Finally, its tectonic significance, especially inference of the seismogenic fault of the Qiaojia earthquake, was discussed.

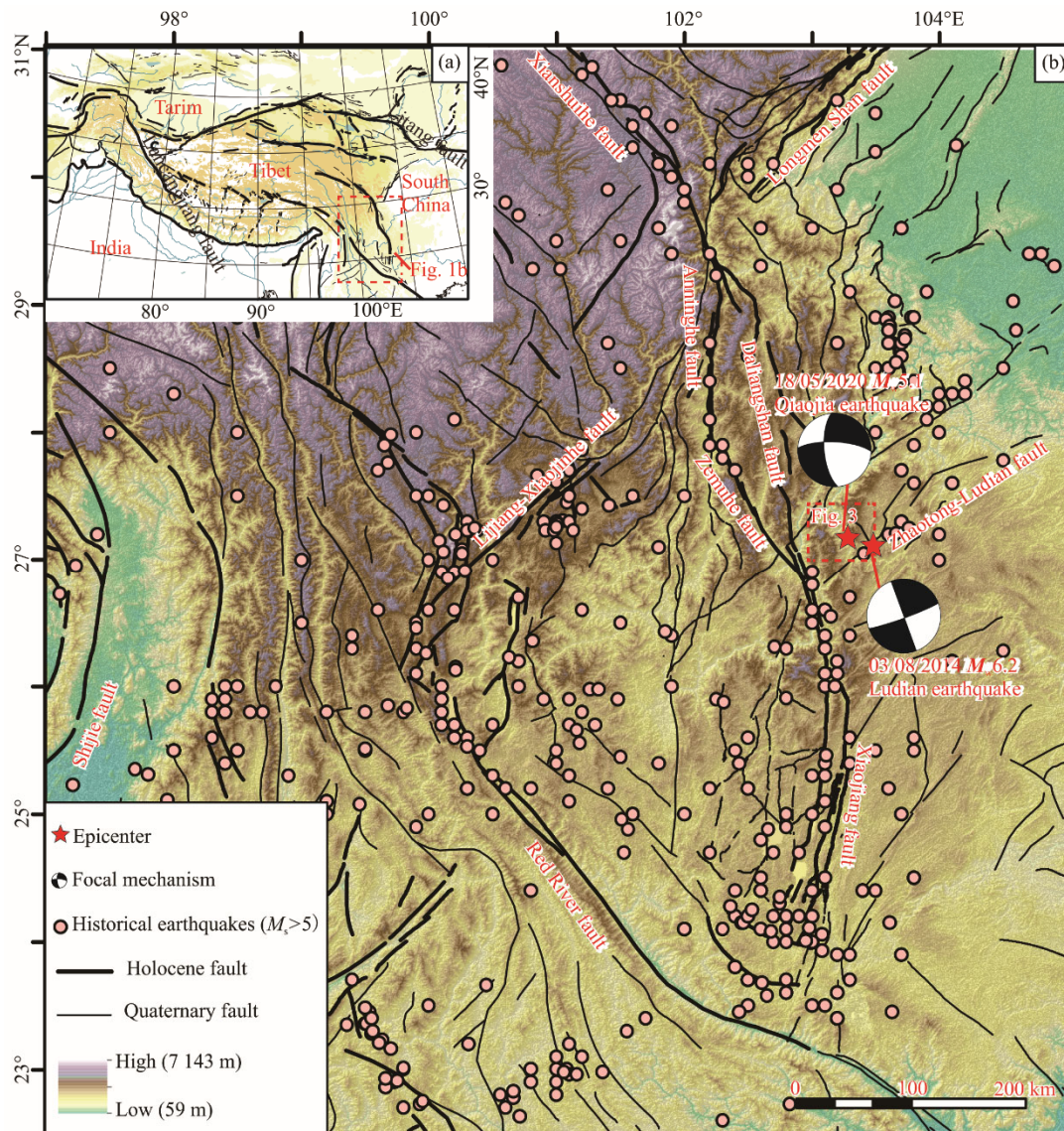


**Figure 1.** Maps showing tectonic setting of the 2020 Qiaojia earthquake. (a) The simplified tectonic map of Tibetan Plateau and adjacent regions. Red dashed box is range of (b); (b) the tectonic setting and historical earthquakes ( $M_s > 5$ ) of Sichuan-Yunnan rhomb block in southeastern margin of Tibetan Plateau. Dashed red box shows scope of Fig. 3 as the study area.

## 1 GEOLOGIC SETTING

The Qiaojia earthquake occurred at 27.18°N, 103.16°E with a focal depth 10 km. The focal mechanism solutions of this event show the strike, dip, and rake of the two nodal planes are 170°/70°/-10° and 263°/81°/-160°, respectively. Its epicenter is ~20 km to the 2014  $M_w$ 6.2 Ludian earthquake that is a conjugated strike-slip event with the main rupture plane on a NNW-trending fault (Cheng et al., 2015; Xu et al., 2015). The 2020 Qiaojia earthquake and 2014 Ludian earthquake both occurred on the western section of the Zhaotong-Lianfeng fault zone and east of the Xianshuihe-Xiaojiang fault zone between the Sichuan-Yunnan rhomb block and the South China Block (Fig. 1; Ren et al., 2010; Shen et al., 2005; Deng et al., 2003; Xu et al., 2003; Zhang et al., 2003; Wang et al., 1998).

Associated with the eastward crustal extrusion of the Tibetan Plateau, the Sichuan-Yunnan region hosts many active faults which generate major earthquakes (Gan et al., 2007). Here the Xianshuihe-Anninghe-Zemuhe-Xiaojiang (XAZX) fault zone is a sinistral strike-slip fault system with high slip rate of ~10 mm/yr (Xu et al., 2003) and frequent earthquakes recorded (Fig. 1, Wen et al., 2008). The Anninghe-Zemuhe fault with slip rate of ~6.5 mm/yr and the Daliangshan fault with slip rate of ~3.5 mm/yr are in the middle segment of the XAZX fault zone. (He et al., 2008; Xu et al., 2003). The slip rate of the Xianshuihe fault is distributed onto the above two faults. The NS-trending faults west to the Daliangshan fault all have the slip rate <1 mm/yr, except for the Mabian fault with the thrust slip of 1.5–2 mm/yr and dextral slip of ~1.1 mm/yr (Ma et al., 2005). There are also two parallel NE-trending faults in this area, i.e., the Lianfeng fault and the Zhaotong fault. These two faults have a low right-lateral slip rate (1–3 mm/yr) with a thrust component (4–6 mm/yr in the southwest to 2–3 mm/yr in the northeast), and the seismic activities of these two faults are relatively lower than the NNW-trending faults (Wen et al., 2013). The 2020  $M_w$ 5.1 Qiaojia earthquake is located in the area where the NNW-trending sinistral faults and the NE-trending dextral faults co-exist. It is also located on the border between the Daliangshan sub-block and the stable South China Block (Chang et al., 2014).

This region has been struck by many moderate-sized earthquakes in recent years, such as the  $M_s$ 5.0 and 5.1 Ludian earthquakes in 2003,  $M_s$ 5.6 Ludian earthquake in 2004,  $M_s$ 5.1 Yanjin earthquake in 2006,  $M_s$ 5.7 and 5.6 Yiliang earthquakes in 2012,  $M_s$ 5.3 and 5.0 Yongshan earthquakes, and  $M_s$ 6.5 Ludian earthquake in 2014. In the history, the two greatest events, the 1974  $M_7.1$  North Daguang and the 1216  $M_s$ 7.0 Mahu earthquakes, occurred at inter sections between the Mabian fault and the Zhaotong-Lianfeng fault (Han et al., 2009; Zhang et al., 1994; Zhu and Chen, 1976). In addition, the Daliangshan fault is a relatively young structure without records of historic earthquakes greater than  $M_s$ 6.5 (He et al., 2008; Xu et al., 2003).

This area was a relatively intact peneplain before Miocene time and has evolved into a mountainous landscape due to many times of tectonic movements since the end of Miocene. In the study area, the strata of the Sinian, Cambrian, Ordovician, Silurian, Devonian, Permian, Neogene, and Quaternary are exposed, while Mesozoic and Carboniferous formations are not seen. The area of Permian strata is largest, dominated by limestone and basalt. The Neogene strata (conglomerate and clay rock) and

Quaternary sediments (clay, sand, gravel and silt loam) are sporadically distributed in the study area. Devonian and Silurian strata crop out in bands, mainly including quartz sandstone, mudstone, siltstone with argillaceous shale, and argillaceous limestone and dolomite. Ordovician and Cambrian strata developed in a relatively vast area, dominated by dolomite and shale with siltstone. Sinian strata appear in the southeast and northwest of the Qiaojia epicenter, with quartz sandstone, dolomite and phyllite (Chang et al., 2016; Geological and Mineral Bureau of Yunnan Province, 1990).

## 2 DATA AND METHODS

### 2.1 Data

Immediately after the 2020 Qiaojia earthquake, a field investigation was undertaken to examine its geologic effects including co-seismic landslides. Meanwhile post-quake satellite images were compared to pre-quake ones to identify slope failure by the shaking. These satellite images were obtained by fusing Gaofen multispectral images and Gaofen panchromatic images. The multispectral images have four bands of spectra (near-infrared: 0.77–0.89  $\mu\text{m}$ , red: 0.63–0.69  $\mu\text{m}$ , green: 0.52–0.59  $\mu\text{m}$ , blue: 0.45–0.51  $\mu\text{m}$ ). Gaofen panchromatic images have only one band of spectra (0.45–0.90  $\mu\text{m}$ ) with a resolution of 0.8–2 m. The fusion images retain four bands of spectra with resolution of 0.8–2 m, which permitted to recognize small landslides and produce a high-quality inventory map. The pre-quake images were acquired between February 7 and May 15, 2020 and post-quake images were acquired between May 19 and May 20, 2020, close to the occurrence time of the Qiaojia earthquake, which permitted to effectively distinguish the coseismic landslides and the landslides already existing before the earthquake. The images covered an area exceeding ~1 410 km<sup>2</sup> in the study area.

In this study, three types of factors, including topography (elevation, and slope angle, aspect and curvature), seismology (seismic intensity and the distance to the Qiaojia earthquake epicenter) and geology (vertical and parallel distances to the Xiaohe-Baogunao fault, and strata lithology), were considered in statistics of the 2020 Qiaojia earthquake landslides. Topography factors were extracted from the digital elevation model (DEM) with a 90-m resolution from Shuttle Radar Topography Mission (SRTM, <http://www.gscloud.cn/search>). Stratum and fault data were extracted from a 1 : 200 000 geological map (Geological and Mineral Bureau of Yunnan Province, 1990).

### 2.2 Methods

Based on the site survey and visual interpretation of satellite images, a coseismic landslide inventory of the Qiaojia event was prepared using the common procedures (Xu C, 2015a). In the process of visual interpretation, first, satellite images are precisely geographically registered on ArcGIS platform; then landslides are identified by comparing the color and vegetation differences between pre- and post-quake images with true-color composite, combining the characteristics of landslides observed in the field investigation. In general, a landslide is represented by a point that defines the location of the landslide or delineated as a polygon that depicts the scale of the landslide (Harp and Jibson, 1995). In this work, the landslides were delineated as

some polygons according the shapes of landslides.

The elevation in the study area was classified into 8 grades with a spacing of 500 m. Slope angle was classified into 6 grades with a spacing of  $10^\circ$ . Slope aspect was classified into 9 grades. Specially, the flat area is horizontal with a zero slope (Jeness et al., 2013). Slope curvature, which means the amount that slope is curved, was divided into 6 classes. There were eight ages of strata in the study area, i.e., Quaternary, Neogene, Permian, Devonian, Silurian, Ordovician, Cambrian, and Sinian. Because the XBF is closest to the epicenter, with a 5-km linear distance, vertical distance to the XBF and parallel distance along the XBF were considered as influencing factors with an interval of 2 km, to examine their correlations with the landslide distribution. Additionally, when examining the effect of the 2014 Ludian earthquake, we chose not only Qiaojia earthquake intensity and the distance to the Qiaojia epicenter, but also Ludian earthquake intensity as seismic factors. The buffers were established around the epicenter with a 2 km interval.

The correlations of these factors with the distribution of the coseismic landslides were examined. Furthermore, we identified the most influential factors and inferred the probable seismogenic fault and the relationship between the Ludian earthquake and Qiaojia earthquake through statistical analysis based on Intersect Function in ArcGIS.

### 3 RESULTS

#### 3.1 Landslide Inventory

Based on the field survey, 18 major landslides were positioned, which damaged houses (Figs. 2a, 2b) and blocked roads (Figs. 2c, 2d). All the debris slides occurred on steep slopes along rivers and roads (Figs. 2e, 2f). Under the strong ground motion, many imminent falling rocks with ruptures appeared on hillslopes (Figs. 2g, 2h), threatening the safety at the foot of the mountain.

Combining field investigations with visual interpretation of satellite images, we eventually prepared an inventory with 167 coseismic landslides for the 2020 Qiaojia earthquake. They were distributed in a region of  $\sim 1\,410\text{ km}^2$  (Fig. 3). The total occupied

area of the landslides is only  $1.81 \times 10^5\text{ m}^2$ . According to the relation between the volume and area of landslides ( $V=1.3147 \times A^{1.2085}$ , Xu et al., 2016), the total landslides volume was estimated to be  $2.97 \times 10^6\text{ m}^3$ . The largest landslide is  $8\,345.17\text{ m}^2$ . There are 102 landslides with an area less than  $1\,000\text{ m}^2$ . The LND and LAP of this study region are  $0.013\text{ km}^{-2}$  and  $0.12\%$ , respectively. Figure 4 shows some landslide interpretation cases by comparing post- and pre-earthquake satellite images. These results imply majority of the landslides are small- and medium-scale rockfalls and debris slides.

#### 3.2 Correlation between Landslide Distribution and Influence Factors

We show the correlation of landslides spatial distribution and various factors by LND and LAP. Using above two indexes, the distribution pattern of the landslides triggered by the 2020 Qiaojia event were characterized by statistics with aforementioned influence factors.

##### 3.2.1 Topographic factors

The elevation in the study area ranges from 513 to 4 026 m. The peaks of LAP and LND both appear in the range of 1 000–1 500 m with values of  $0.038\%$  and  $0.3\text{ km}^{-2}$ , respectively (Figs. 5a, 5b). There are  $\sim 33\%$  of the total landslides occurred within  $\sim 13\%$  of areas with elevations of 1 000 to 1 500 m in the study area. The values of LND in the ranges of  $<1\,000$ , 1 500–2 000, 2 000–2 500 and 2 500–3 000 m are all about  $0.1\text{ km}^{-2}$ , and those in the ranges of 3 000–3 500, 3 500–4 000 and  $>4\,000$  m are smaller further. The curvilinear tend of LAP is generally consistent with that of LND for the elevation factor (Fig. 5b).

The slope angle ranges  $0\text{--}76.7^\circ$ , and the areas of each class decrease with increase of the slope angle in the study area. The LAP has generally positive correlations with the slope angles, while the LND firstly increases with the growing slope angle and then decreases from  $50^\circ\text{--}60^\circ$  (Figs. 5c, 5d). The range with slope angles greater than  $60^\circ$  has the largest LAP and the smallest LND, which is attributed to individual large landslides.



**Figure 2.** Pictures showing landslide hazards during 2020 Qiaojia earthquake. (a) and (b) damaged houses by rockfalls; (c) and (d) blocked roads by rockfalls; (e) and (f) debris slides; (g) and (h) imminent falling rocks with ruptures.

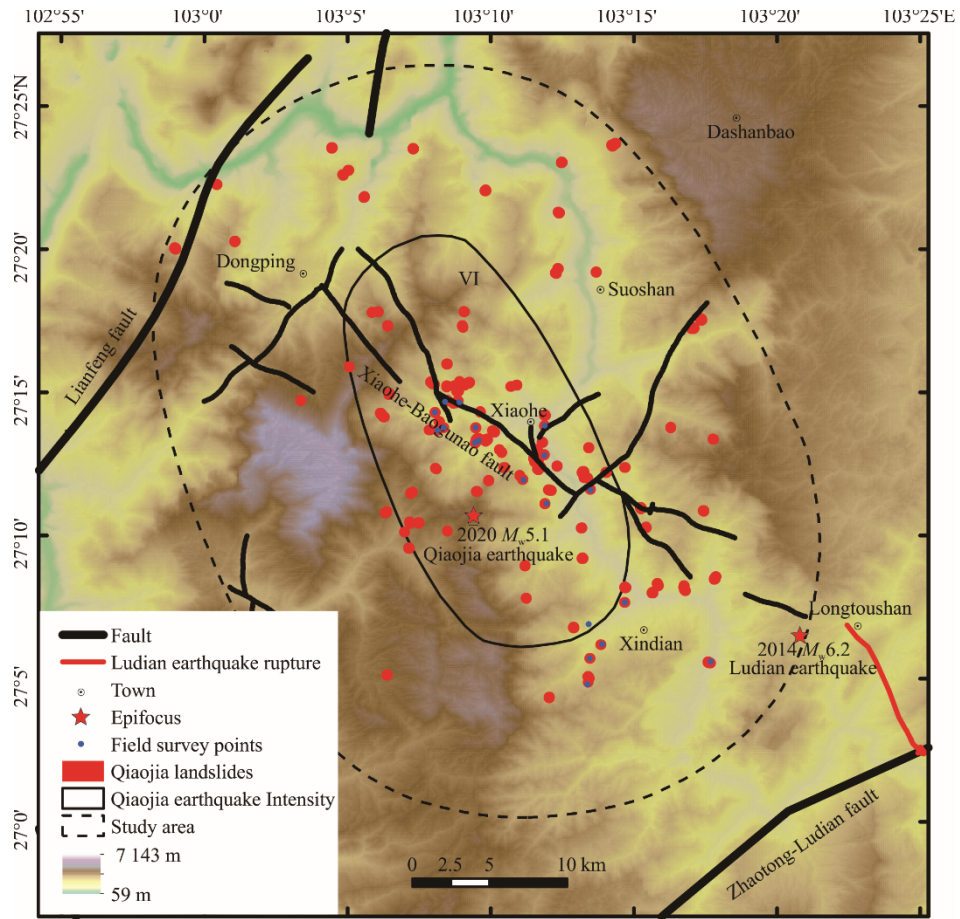


Figure 3. Map showing study area (dashed ellipse) and distribution of landslides by the 2020 Qiaojia earthquake.

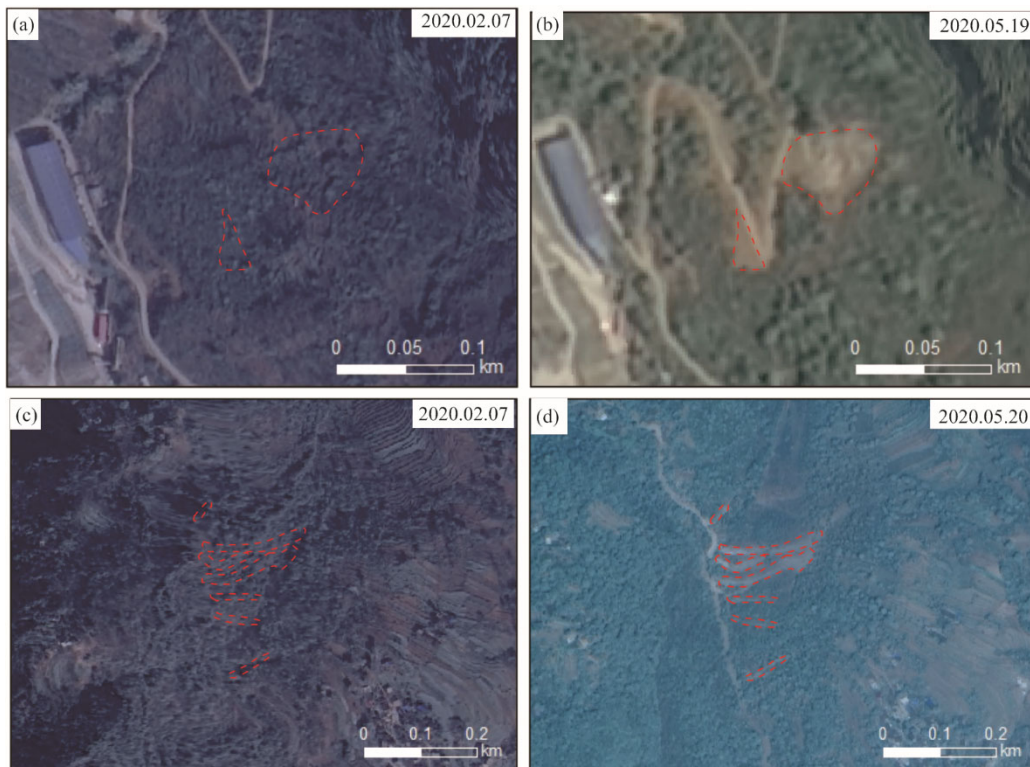
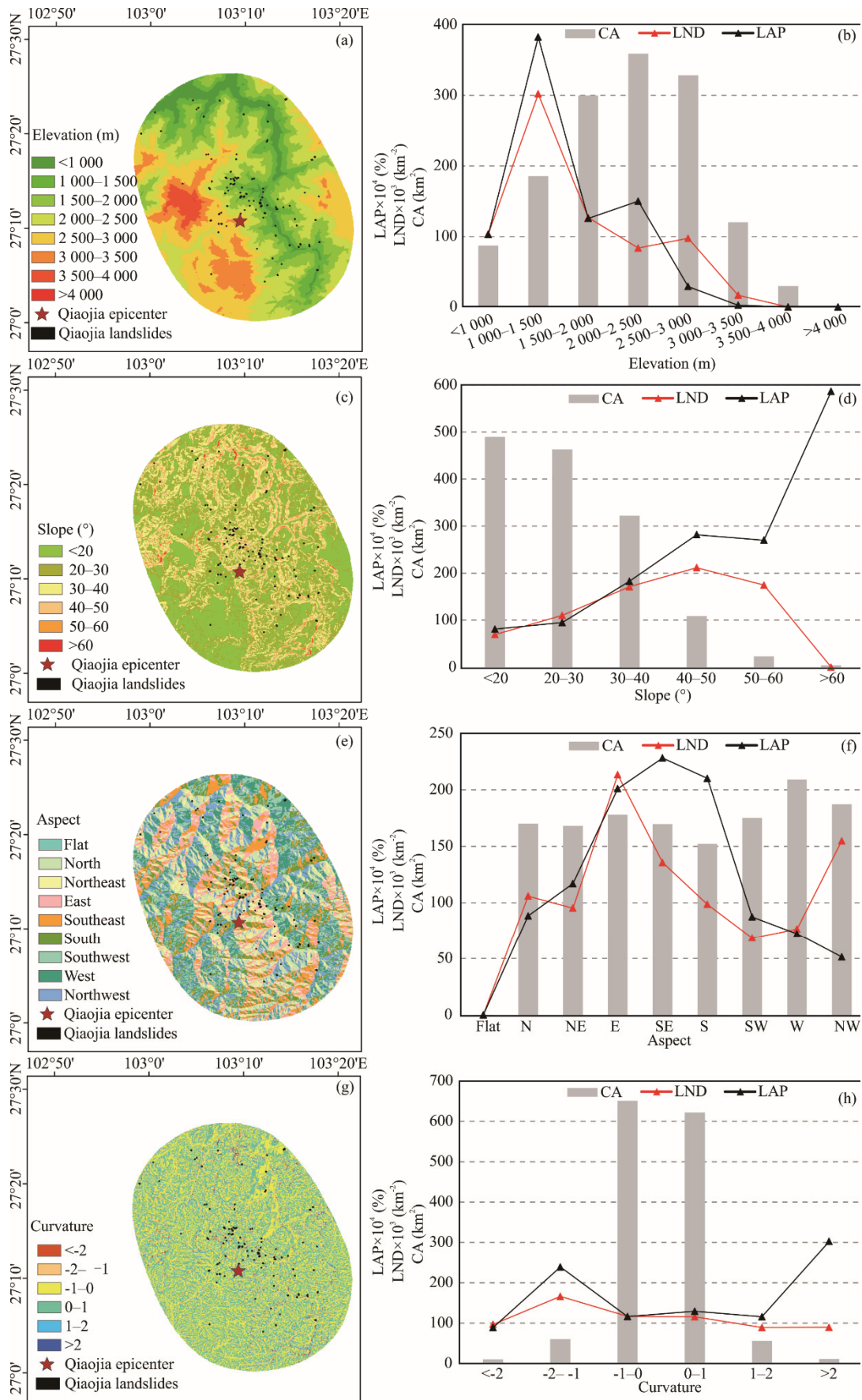


Figure 4. Two representative cases of landslides from interpretation by comparing post- and pre-earthquake satellite images. Pre-earthquake ones were acquired on February 7, 2020, and post-earthquake ones on May 19 or 20, 2020. Red dotted lines show identified landslides.



**Figure 5.** The landslide distribution in classifications of topographical factors (left) and their correlations (right) described by LAP and LND. LAP. Landslide area percentage; LND. landslide number density; CA. classification area.

The area of each class of the slope aspect is relatively mean, except the flat aspect that is almost nothing. The peak of LND is on the east-facing slopes, followed by that on the southeast- and northwest-facing slopes, while the LAP on the south-, southeast- and east-facing slopes are obviously larger than other aspects (Figs. 5e, 5f). It means that the scales of landslides on south-facing slopes are relatively larger than those on northwest-facing slopes.

Slope curvature is also a topographic factor affecting the distribution of landslides. Negative curvature indicates a concave slope and positive curvature indicates a convex slope. A slope, with zero or near zero curvature, is a straight plane. As shown in Figs. 5g, 5h, most of the slopes are on straight slopes. The LAP and LND in the range of -2– -1 of the curvature are

slightly larger. The larger LAP in the range of >2 of the curvature is due to individual landslides with relatively large area. It seems that there is almost no correlation between landslide distribution and slope curvature.

### 3.2.2 Geologic factors

As shown in Figs. 6a and 6b, the Permian strata dominated by limestone and basalt take up the largest area in the study area, with few landslides. The LND and LAP both are relatively larger in Ordovician and Cambrian strata (Figs. 6a, 6b), the lithologies of which are characterized by more dolomite and shale with siltstone. However, it is hard to clarify whether this is due to different lithologies, because other strata also contain dolomite and siltstone.

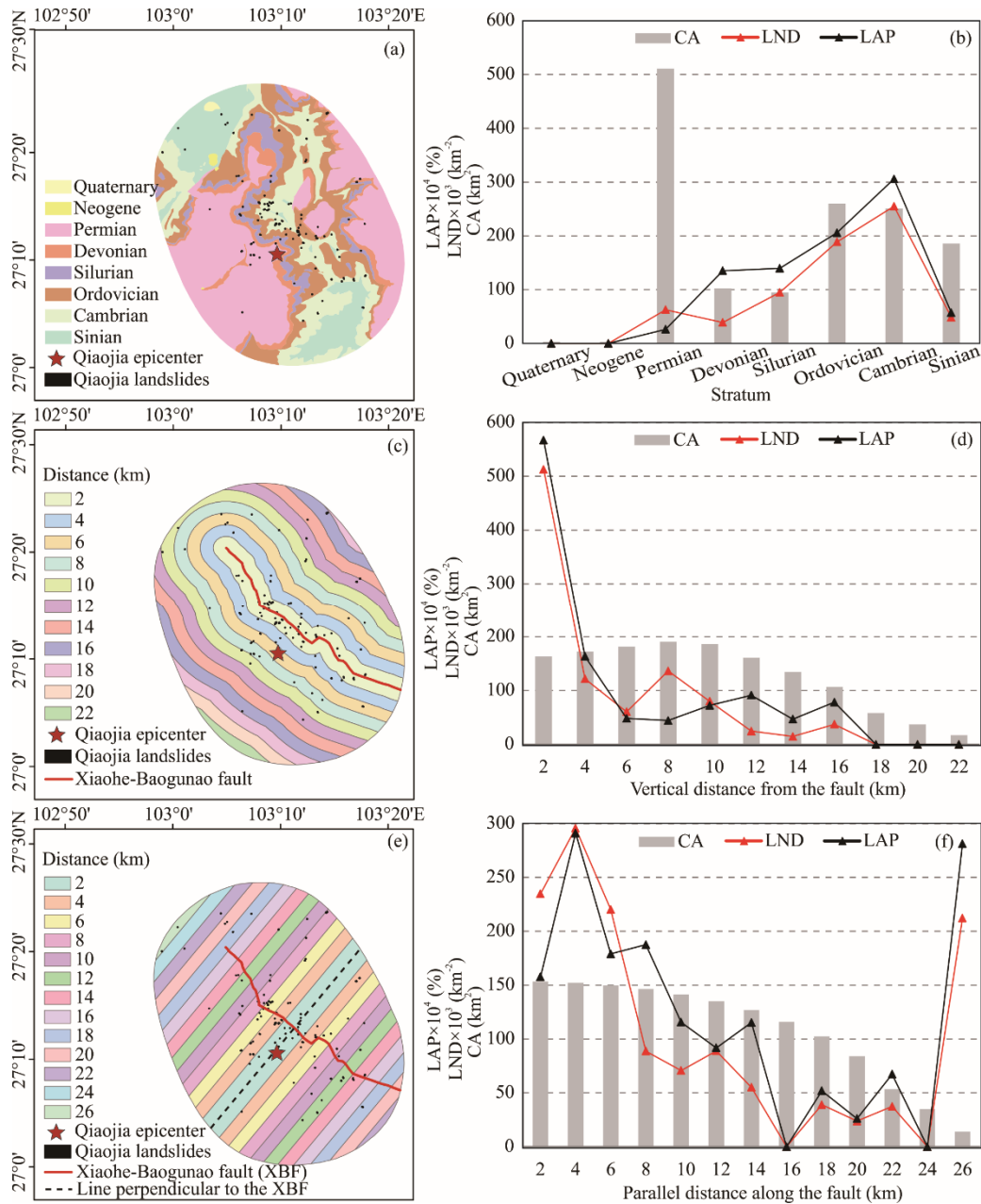


**Figure 6.** Landslide distribution in categories of geological factors (left) and their correlations (right). (a) and (b) stratum; (c) and (d) vertical distance from the Xiaohe-Baogunao fault (XBF); (e) and (f) parallel distance along the Xiaohe-Baogunao fault (XBF). LAP. Landslide area percentage; LND. landslide number density; CA. classification area.

Figures 6c and 6d show the landslide distribution in the bands parallel to the Xiaohe-Baogunao fault (XBF) (location shown in Fig. 3). Obviously, the landslides concentrate on both sides of the fault. The LAP and LND generally decrease as the vertical distance to the fault increases, though there are some small fluctuations. Their peaks occur in the band with distance less than 2 km from the fault, with values of 0.51 km<sup>2</sup> and 0.057%, respectively.

The LAP and LND in the strips vertical to the XBF are displayed in Figs. 6e, 6f, which indicate the landslide distribution varies along the fault. The most of landslides are present in the strips close to the epicenter (within 6 km) and the peaks of LND and LAP are in the band within distance 2–4 km to the epicenter. From the distance of 4 km, the scale and number of

landslides generally decrease as the distance from the epicenter increases. The LND and LAP sharply increase in the largest distance, which may attributed to the stress concentration effect at fault ends, or because of the small classification area in statistics.

### 3.2.3 Seismic factors

Figures 7a and 7b show the most landslides occurred within 2–8 km to the epicenter instead of the proximity area. Particularly, the range of 4–6 km to the epicenter has the largest LAP and LND values. From the distance of 6 km, the scale and number of landslides generally decrease as the distance from the epicenter increases, while the values in the range of 0–2 km to the epicenter are smaller than those in the range of 8–10 km.

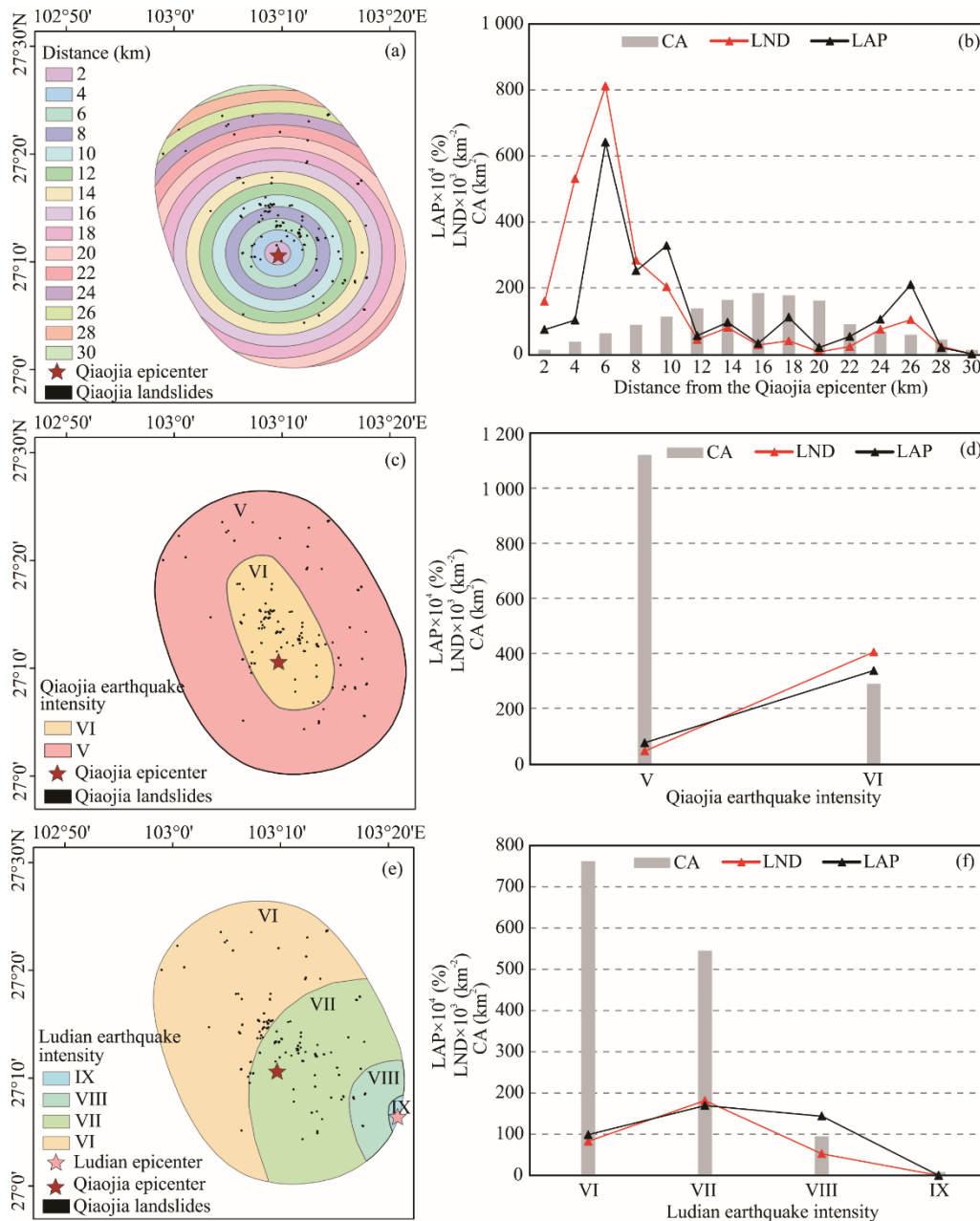


**Figure 7.** Landslide distribution in categories of seismic factors (left) and their correlations (right). (a) and (b) distance from the epicenter of Qiaojia earthquake; (c) and (d) intensity of Qiaojia earthquake area; (e) and (f) Ludian earthquake intensity. LAP, Landslide area percentage; LND, landslide number density; CA, classification area.



Apparently, the scale and number of landslides in the VI degree zone of the Qiaojia earthquake intensity are dominant, although the area of the V degree zone is obviously larger than that of the VI degree zone (Figs. 7c, 7d). In the study area, the classification areas decrease with increase of the Ludian earthquake intensity, while the LND and LAP in the VII degree zone of the Ludian earthquake intensity are slightly larger than other zones (Figs. 7e, 7f).

## 4 DISCUSSION

### 4.1 Influence Factors of Landslide Occurrence

In this work, the distribution pattern of the landslides induced by the 2020 Qiaojia earthquake was characterized concerning varieties of influence factors. Among topographical factors, most landslides occurred in the regions with elevations of 1 000 to 1 500 m (Figs. 5a, 5b), but these areas have no distinctive features that can affect the occurrence of landslides. The LAP and LND seem to increase with the increasing slope angles, which is likely attributed to that the area of each grade reduces with increase of the slope angle (Figs. 5c, 5d). It is clear that there is almost no correlation between landslide distribution and slope curvature (Figs. 5g, 5h). Uniquely, the number or scale of landslides on E-, SE-, and S-facing slopes is relatively larger (Figs. 5e, 5f), which probably resulted from the effect of previous earthquakes (this will be discussed in section 4.3).

For geological factors, according to variations of the LAP and LND in different strata and the detail of stratigraphic lithology (Figs. 6a, 6b), it is hard to see the relationship of lithology and landslides occurrence. However, it is obvious that the Xiaohe-Baogunao fault is closely related to landslide occurrence; the landslides concentrate on two sides of the fault (Figs. 6c and 6d) and the number and scale generally decrease from the epicenter to fault ends (Figs. 6e, 6f).

For seismic factors, the landslides are mainly distributed near the epicenter (Figs. 7a, 7b) and within the zone of maximum seismic intensity of the Qiaojia earthquake (Figs. 7c, 7d). What calls for special attention is the correlation between the 2014 Ludian earthquake intensity and landslide occurrence; most landslides are in the VII degree intensity zone of the 2014 Ludian earthquake (Figs. 7c, 7d), where the damages are relatively serious by the Ludian and Qiaojia earthquakes.

### 4.2 Seismogenic Fault of the Qiaojia Earthquake

There are many methods to infer seismogenic faults, each has its own advantages and disadvantages. In seismic moment tensor inversion, two possible fault planes (nodal planes) corresponding to the best double couple can be obtained, but it is difficult to confirm which one is the real seismogenic fault. While it is possible to confirm the seismogenic fault according to the waveform residuals from inversion based on trying two couple nodal planes one by one (Zhang Y et al., 2014). In general, the seismogenic fault can be identified by combination of focal mechanism solutions, aftershock distribution, and seismic ruptures on the surface. Such an approach is suitable for large earthquakes because of the clear fault parameters, obvious band-like distribution of aftershocks, and the large rupture length (Zhang Y et al., 2014). In general, it is difficult to determine the seismogenic fault of medium-sized earthquakes. First, medium-sized

earthquakes are likely to occur on secondary or small faults, and usually cannot produce surface ruptures visible. Second, preliminary positioning of the aftershocks of such earthquakes is often scattered, easy to blur the direction of rupturing. And third, the signal-to-noise ratio of medium-sized earthquakes at teleseismic distances is low, thus difficult to distinguish the rupture direction.

For the 2020  $M_w5.1$  Qiaojia earthquake, the strike, dip, and rake of the two nodal planes are  $170^\circ/70^\circ/-10^\circ$  and  $263^\circ/81^\circ/-160^\circ$ , respectively, according to focal mechanism solutions from China Earthquake Networks. The seismic intensity map of this event released by the Yunnan Seismological Bureau shows elliptical isoseismal lines with a long axis striking SSE160° (Fig. 3). Zhao et al. (2020) used the horizontal peak ground acceleration (PGA) values recorded by stations near Qiaojia to perform geometric averaging, yielding horizontal PGA contours spreading in the NW-SE direction. The peak acceleration reduces as the distance to the epicenter increases, of which variation tendency has a strong similarity to the trend of the seismic intensity map prepared by the Yunnan Seismological Bureau. Li et al. (2020) showed that the aftershock distribution within 24 h after the mainshock of the Qiaojia event has a long axis in SSE175°, which largely accords with the SSE nodal plane in the focal mechanism solutions and the long axis direction of the seismic intensity contours. With these constraints, it is inferred that source rupture of the Qiaojia earthquake should be the nodal plane (strike  $170^\circ$ , dip angle  $70^\circ$ , slip angle  $-10^\circ$ ) with sinistral strike-slip. Among the faults around the epicenter of the 2020 Qiaojia  $M_w5.1$  earthquake, the XBF is the closest, with a straight distance of only 5 km, which trends in NW. According to the 1 : 200 000 regional geological map of the Ludian Sheet, the fault trace is not continuous, and there are many secondary echelon faults with an acute angle on two sides of the main fault zone, and the motion of the XBF is mainly sinistral strike-slip (Cheng et al., 2015; Xu et al., 2015).

Superposing the magnitude and the distribution area of landslides for the Qiaojia earthquake on the map showing correlation between the distribution area of coseismic landslides with the magnitude (Xu et al., 2014b), we found that the distribution area of the Qiaojia coseismic landslides is larger than that of the events with same magnitude, while the 2014 Ludian earthquake is within the envelope (Fig. 8a). From the diagram showing the correlation between the magnitude and the number of coseismic landslides (Alfaro et al., 2012; Keefer, 2002), the number of the Qiaojia coseismic landslides is greater than that of the earthquakes with same magnitude, while the Ludian earthquake are close to the fitted line (Fig. 8b). Combining the results of field investigations and remote sensing interpretation, it is clear that the Qiaojia earthquake landslides are large in number, small in scale, and distributed in a large area, and the overall distribution is in the NW-SE direction (Fig. 3). Based on the analysis of the correlation between the landslide distribution and fault factors of this earthquake (Figs. 6b, 6c, 6e and 6f), the landslides mainly occurred symmetrically along both sides of the XBF, decreasing with the increasing distance from the fault, and gradually decrease along the fault from the epicenter to both ends of the fault. Based on the aforementioned relationship between the seismogenic fault and coseismic landslides distribution, combined with the nodal planes of focal mechanism, seismic intensity, PGA

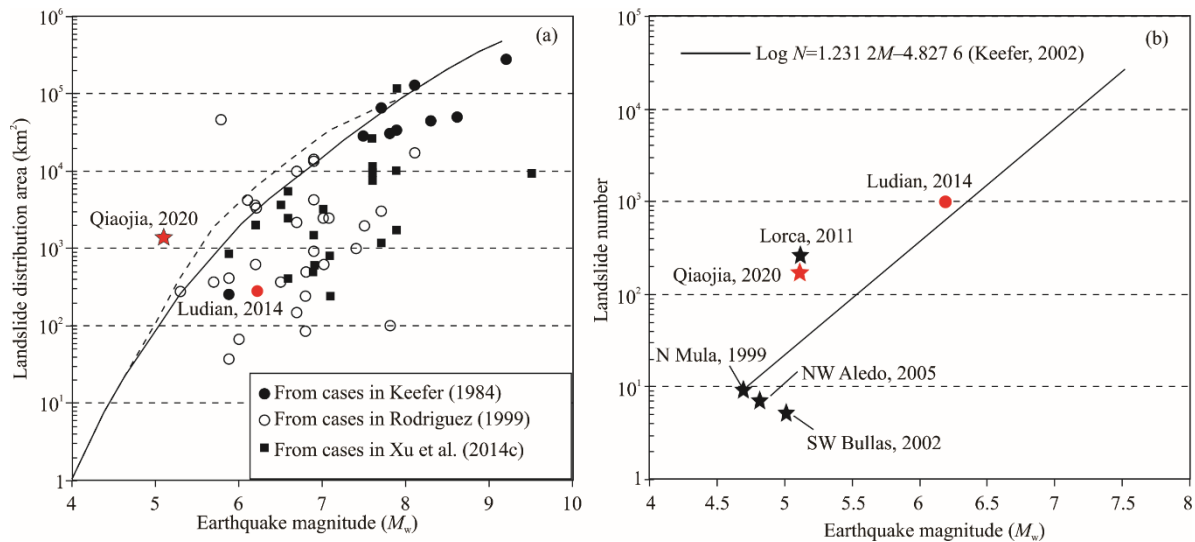


**Figure 8.** The distribution area and number of landslides induced by 2020 Qiaojia earthquake compared with other events. (a) The relationship between the earthquake magnitude and the landslides distribution area (modified from Xu et al., 2014b); (b) the correlation between the earthquake magnitude and the landslides number (modified from Alfaro et al., 2012).

contours, and the predominant direction of aftershocks, it is inferred that the XBF has a close correlation with this earthquake. However, considering the small difference among nodal planes of the Qiaojia earthquake, the long axis trend of the isoseismal line, the dominant earthquake sequence tendency and the main strike of the XBF, we suggest that the seismogenic structure of the Qiaojia earthquake may be an echelon-shaped secondary and buried fault branch of the XBF.

### 4.3 The Relationship between the Qiaojia Earthquake and Ludian Earthquake

The epicenter of the 2020  $M_w$ 5.1 Qiaojia earthquake is only 20 km away from the 2014  $M_w$ 6.2 Ludian earthquake. The landslides by the Qiaojia event are all within the VI–VIII degree zones of the Ludian earthquake intensity, mostly in the VII zone. The focal mechanism solutions of the Ludian event (Chen et al., 2020b; Xie et al., 2015; Zhang G W et al., 2014) show a nodal plane with  $162^\circ/70^\circ/-14^\circ$  (according to Global GMT), which is similar to that of the Qiaojia earthquake ( $170^\circ/70^\circ/-10^\circ$ ). The Qiaojia earthquake landslides are largely distributed on the SE- and E-facing slopes and the scales of the landslides on the S- and SE-facing slopes are relatively large (Figs. 5c, 5g). The slopes facing these directions may be affected by the 2014 Ludian earthquake in the southeast. Additionally, all of the Qiaojia earthquake landslides happened in the region with the intensity greater than six degrees of the seismic intensity of the Ludian earthquake; particularly in the VII intensity zone (Figs. 7e, 7f), where the damages were probably maximally superimposed by the Ludian and Qiaojia earthquakes. The strip-like distribution of aftershocks in the  $N30^\circ W$  direction, the long axis of intensity (IX) zone in NNW-NW-direction, and seismic ruptures in the episeismic zone suggest that the 2014 Ludian earthquake's seismogenic fault is also the NW-trending XBF (Cheng et al., 2015; Xu Z J et al., 2015; Wang et al., 2014; Xu X W et al., 2014). The focal mechanism solutions indicate that the seismogenic fault of the Ludian event is dominated by sinistral strike-slip, with a small normal faulting component (Xu L S et al., 2014; Zhang G W et

al., 2014), which accords with the 2020 Qiaojia earthquake. These imply that the 2020  $M_w$ 5.1 Qiaojia earthquake may be related to the 2014 Ludian  $M_w$ 6.2 earthquake.

Xu et al. (2014b) used the elastic mid-space model (Okada, 1992) and the coseismic kinematics data of the XBF to calculate the Coulomb stress change at the depth of 10 km caused by the 2014 Ludian earthquake. The results show that the increase of static Coulomb stress is most obvious in an around 70% area near the XBF, up to 70 kPa. Miao and Zhu (2016) obtained the similar results. Most of the aftershocks of the Ludian event are in the region of increased Coulomb stress resulting from the main earthquake, implying the Ludian earthquake has a triggering effect on the subsequent aftershocks (Fig. 9). According to previous work, the 2014 Ludian earthquake expanded from the

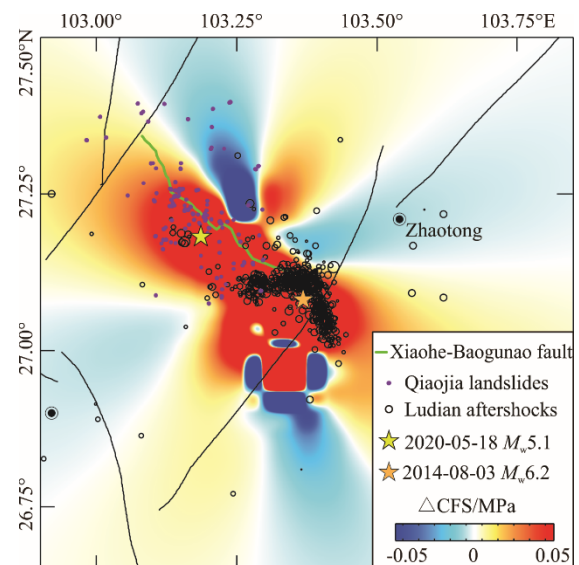


**Figure 9.** Map showing landslides triggered by 2020  $M_w$ 5.1 Qiaojia earthquake, epicenters, seismogenic fault, and static Coulomb stress change and aftershock distribution of 2014  $M_w$ 6.2 Ludian earthquake (modified from Miao and Zhu, 2016).

deep to the shallow crust in the SSE direction, and a seismic surface rupture appeared in the southeast of the XBF (Xu X W et al., 2014). The 2020 Qiaojia earthquake epicenter and the most of coseismic landslides are located in the north-central section of the XBF where the static Coulomb stress has increased significantly, which might result from the 2014 Ludian earthquake event (Fig. 9). The distribution direction of the Qiaojia earthquake-induced landslides is overall consistent with that of aftershocks of the Ludian earthquake in SE-NW direction, while the former seems to be the extension of the later development toward northwest (Fig. 9).

Both the 2014 Ludian and the 2020 Qiaojia earthquakes happened in the southeast of the Qiangtang Block and the east border of the Sichuan-Yunnan rhomb block, with the sinistral strike-slip XBF in the east of the XAZX fault zone. The XBF is a secondary active fault near the main boundary fault zone of the Sichuan-Yunnan rhomb block, which has not been noticed before the earthquakes. These two events may indicate that the Sichuan-Yunnan rhomb block, especially the central Yunnan sub-block, continuously moves to SE, leading to continuous accumulation of elastic strain in the block boundary zones and their vicinity. Because the scale of the secondary active faults is small, and its earthquake-generating capacity is relatively weak, the earthquakes produced by them are often medium-sized. Therefore, although we cannot assert that the 2020  $M_w$ 5.1 Qiaojia earthquake is an aftershock of the 2014  $M_w$ 6.2 Ludian earthquake, it can be inferred that the Qiaojia earthquake is the subsequent release of the stress accumulation after the 2014 Ludian earthquake under the background that the rhomb block keeps moving towards SE. The reason why the landslide hazard induced by the Qiaojia earthquake is more serious than others with the similar magnitude is probably due to the effect of the 2014 Ludian earthquake on the stability of the slopes in this area.

## 5 CONCLUSIONS

Based on field investigations, visual interpretation of remote sensing images based on ArcGIS, a detailed inventory of the landslides induced by 2020  $M_w$ 5.1 Qiaojia, Yunnan China earthquake was prepared. The correlation of spatial distribution with possible influence factors involving topography, geology and seismology and tectonic significance of these landslides were studied. The conclusions are as follows.

(1) In total, 167 coseismic landslides of the 2020 Qiaojia earthquake were delineated, with a distribution area of  $\sim 1$  410 km<sup>2</sup> and landslide-occupation area of 0.18 km<sup>2</sup>, respectively. They are distributed in a relatively broad area, smaller on the scale for individuals and larger in the number compared to those of other events with same magnitude.

(2) For topographical factors, the number and scale of landslides on S-, SE-, and E-facing slopes are relatively larger. For geological factors, the correlation between faults and landslide occurrence is more significant than that between stratum lithology and landslide occurrence. The LAP and LND generally reduce with increasing vertical distance from the fault, and gradually reduce from the epicenter to both ends of the Xiaohe-Baogunao fault. For seismic factors, landslides are mostly concentrated near the epicenter and within the zone of maximum seismic intensity. Meanwhile it is noted that all the landslides are

in the VI–VIII degree zones of intensity map of the 2014 Ludian earthquake.

(3) Combining landslide distribution, the long axis of the maximum intensity zone, aftershocks, PGA, and focal mechanism solutions, it is inferred that the seismogenic structure of the 2020 Qiaojia earthquake is likely a secondary hidden structure of the Xiaohe-Baogunao fault (XBF). Under the regional seismotectonic background, the 2020 Qiaojia earthquake may be the inheritance of the 2014 Ludian earthquake in stress release. The relatively serious geohazard by the Qiaojia event is probably associated with the aftermath of the 2014 Ludian earthquake.

## ACKNOWLEDGMENTS

This work was supported by the National Natural Science Foundation of China (No. 42077259) and the National Institute of Natural Hazards, Ministry of Emergency Management of China (No. ZDJ2019-31). We thank Shoubiao Zhu for providing us an original view of Fig. 9. We wish to thank the associate editors and two anonymous reviewers for their useful suggestions to improve the manuscript. The final publication is available at Springer via <https://doi.org/10.1007/s12583-021-1492-1>.

## REFERENCES CITED

- Alfaro, P., Delgado, J., García-Tortosa, F. J., et al., 2012. Widespread Landslides Induced by the  $M_w$ 5.1 Earthquake of 11 May 2011 in Lorca, SE Spain. *Engineering Geology*, 137/138: 40–52. <https://doi.org/10.1016/j.enggeo.2012.04.002>
- Chang, Z. F., Chen, X. L., An, X. W., et al., 2016. Contributing Factors to the Failure of an Unusually Large Landslide Triggered by the 2014 Ludian, Yunnan, China,  $M_s=6.5$  Earthquake. *Natural Hazards and Earth System Sciences*, 16(2): 497–507. <https://doi.org/10.5194/nhess-16-497-2016>
- Chang, Z. F., Zhou, R. J., An, X. W., et al., 2014. Late-Quaternary Activity of the Zhaotong-Ludian Fault Zone and Its Tectonic Implication. *Seismology and Geology*, 36(4): 1260–1279 (in Chinese with English Abstract)
- Chen, J. L., Zheng, Y., Zhang, L., et al., 2020b. Focal Mechanism Solutions of the 2014 Ludian  $M_s$ 6.5 Earthquake Sequence Derived from Multiple-Bandwidth Waveform Fitting. *Chinese Journal of Geophysics*, 63(4): 1472–1483 (in Chinese with English Abstract)
- Chen, S., Miao, Z. L., Wu, L. X., et al., 2020. Application of an Incomplete Landslide Inventory and One Class Classifier to Earthquake-Induced Landslide Susceptibility Mapping. *IEEE Journal of Selected Topics in Applied Earth Observations and Remote Sensing*, 13: 1649–1660. <https://doi.org/10.1109/JSTARS.2020.2985088>
- Cheng, J., Wu, Z., Liu, J., et al., 2015. Preliminary Report on the 3 August 2014,  $M_w$ 6.2/ $M_s$ 6.5 Ludian, Yunnan-Sichuan Border, Southwest China, Earthquake. *Seismological Research Letters*, 86(3): 750–763. <https://doi.org/10.1785/0220140208>
- Cui, Y. L., Bao, P. P., Xu, C., et al., 2021. Landslides Triggered by the 6 September 2018  $M_w$ 6.6 Hokkaido, Japan: An Updated Inventory and Retrospective Hazard Assessment. *Earth Science Informatics*, 14(1): 247–258. <https://doi.org/10.1007/s12145-020-00544-8>
- Dai, F. C., Tu, X. B., Xu, C., et al., 2011. Rock Avalanches Triggered by Oblique-Thrusting during the 12 May 2008  $M_s$ 8.0 Wenchuan Earthquake, China. *Geomorphology*, 132(3/4): 300–318. <https://doi.org/10.1016/j.geomorph.2011.05.016>
- Deng, Q. D., Zhang, P. Z., Ran, Y. K., et al., 2003. Basic Characteristics of Active Tectonics of China. *Science in China Series D: Earth Sciences*,

- 46(4): 356–372. <https://doi.org/10.1360/03yd9032>
- Fan, X. M., Scaringi, G., Korup, O., et al., 2019. Earthquake-Induced Chains of Geologic Hazards: Patterns, Mechanisms, and Impacts. *Reviews of Geophysics*, 57(2): 421–503. <https://doi.org/10.1029/2018rg000626>
- Gan, W. J., Zhang, P. Z., Shen, Z. K., et al., 2007. Present-Day Crustal Motion within the Tibetan Plateau Inferred from GPS Measurements. *Journal of Geophysical Research Solid Earth*, 112: B08416
- Geological and Mineral Bureau of Yunnan Province, 1990. Regional Geological Map of Yunnan Province. Geological Press, Beijing
- Guzzetti, F., Mondini, A. C., Cardinali, M., et al., 2012. Landslide Inventory Maps: New Tools for an Old Problem. *Earth-Science Reviews*, 112(1/2): 42–66. <https://doi.org/10.1016/j.earscirev.2012.02.001>
- Han, Z., He, Y. L., An, Y. F., et al., 2009. A Newly Generated Seismotectonic Zone—Preliminary Study on the Latest Tectonic Deformation of the Mabian Earthquake Zone. *Acta Geologica Sinica*, 83(2): 218–229 (in Chinese with English Abstract)
- Harp, E. L., Jibson, R. W., 1995. Inventory of Landslides Triggered by the 1994 Northridge, California Earthquake. USGS. <http://geondsi.er.usgs.gov/metadata/openfile/95-213/>
- Harp, E. L., Keefer, D. K., Sato, H. P., et al., 2011. Landslide Inventories: The Essential Part of Seismic Landslide Hazard Analyses. *Engineering Geology*, 122(1/2): 9–21. <https://doi.org/10.1016/j.enggeo.2010.06.013>
- He, H. L., Ikeda, Y., He, Y. L., et al., 2008. Newly-Generated Daliangshan Fault Zone—Shortcutting on the Central Section of Xianshuihe-Xiaojiang Fault System. *Science in China Series D: Earth Sciences*, 51(9): 1248–1258. <https://doi.org/10.1007/s11430-008-0094-4>
- Jenness, J., Brost, B., Beier, P., 2013. Land Facet Corridor Designer: Extension for ArcGIS. Jenness Enterprises. [2018-11-10]. [http://www.jennessent.com/arcgis/land\\_facets.htm](http://www.jennessent.com/arcgis/land_facets.htm)
- Kargel, J. S., Leonard, G. J., Shugar, D. H., et al., 2016. Geomorphic and Geologic Controls of Geohazards Induced by Nepals 2015 Gorkha Earthquake. *Science*, 351(6269): aac8353. <https://doi.org/10.1126/science.aac8353>
- Keefer, D. K., 2002. Investigating Landslides Caused by Earthquakes—A Historical Review. *Surveys in Geophysics*, 23(6): 473–510. <https://doi.org/10.1023/A:1021274710840>
- Khattak, G. A., Owen, L. A., Kamp, U., et al., 2010. Evolution of Earthquake-Triggered Landslides in the Kashmir Himalaya, Northern Pakistan. *Geomorphology*, 115(1/2): 102–108. <https://doi.org/10.1016/j.geomorph.2009.09.035>
- Li, W. T., Dang, W. J., Jin, M. P., et al., 2020. The Focal Mechanism Solution and Seismogenic Fault of the 2020 Qiaojia  $M_s$ 5.0 Earthquake in Yunnan. *Seismological and Geomagnetic Observation and Research*, 41(3): 184–192 (in Chinese with English Abstract)
- Liao, H. W., Lee, C. T., 2000. Landslides Triggered by the Chi-Chi Earthquake. In: Proceedings of the 21st Asian Conference on Remote Sensing, Taipei. 1/2: 383–388
- Ma, B. Q., Su, G., Hou, Z. H., et al., 2005. Late Quaternary Slip Rate in the Central Part of the Longmenshan Fault Zone from Terrace Deformation along the Minjiang River. *Seismology and Geology*, 27(2): 234–242 (in Chinese with English Abstract)
- Miao, M., Zhu, S. B., 2016. The Static Coulomb Stress Change of the 2014 Ludian Earthquake and Its Influence on the Aftershocks and Surrounding Faults. *Seismology and Geology*, 38(1): 169–181 (in Chinese with English Abstract)
- Okada, Y., 1992. Internal Deformation Due to Shear and Tensile Faults in a Half-Space. *Bulletin of the Seismological Society of America*, 82(2): 1018–1040
- Parker, R. N., Densmore, A. L., Rosser, N. J., et al., 2011. Mass Wasting Triggered by the 2008 Wenchuan Earthquake is Greater than Orogenic Growth. *Nature Geoscience*, 4(7): 449–452. <https://doi.org/10.1038/ngeo1154>
- Ren, Z. K., Lin, A. M., Rao, G., 2010. Late Pleistocene-Holocene Activity of the Zemuhe Fault on the Southeastern Margin of the Tibetan Plateau. *Tectonophysics*, 495(3/4): 324–336. <https://doi.org/10.1016/j.tecto.2010.09.039>
- Shao, X. Y., Xu, C., Ma, S. Y., et al., 2019. Effects of Seismogenic Faults on the Predictive Mapping of Probability to Earthquake-Triggered Landslides. *ISPRS International Journal of Geo-Information*, 8(8): 328. <https://doi.org/10.3390/ijgi8080328>
- Shen, Z. K., Lü, J., Wang, M., et al., 2005. Contemporary Crustal Deformation around the Southeast Borderland of the Tibetan Plateau. *Journal of Geophysical Research: Solid Earth*, 110(B11): B11409. <https://doi.org/10.1029/2004jb003421>
- Tian, Y. Y., Xu, C., Ma, S. Y., et al., 2019. Inventory and Spatial Distribution of Landslides Triggered by the 8th August 2017  $M_w$ 6.5 Jiuzhaigou Earthquake, China. *Journal of Earth Science*, 30(1): 206–217. <https://doi.org/10.1007/s12583-018-0869-2>
- Vanani, A. A. G., Shoaie, G., Zare, M., 2021. Statistical Analyses of Landslide Size and Spatial Distribution Triggered by 1990 Rudbar-Manjil ( $M_w$ 7.3) Earthquake, Northern Iran: Revised Inventory, and Controlling Factors. *Bulletin of Engineering Geology and the Environment*, 80(4): 3381–3403. <https://doi.org/10.1007/s10064-021-02106-8>
- Wang, E., Burchfiel, B. C., Royden, L. H., et al., 1998. Late Cenozoic Xianshuihe-Xiaojiang, Red River, and Dali Fault Systems of Southwestern Sichuan and Central Yunnan, China, *Special Paper of the Geological Society of America*, 327: 1–108. <https://doi.org/10.1130/0-8137-2327-2.1>
- Wang, W. L., Wu, J. P., Fang, L. H., et al., 2014. Double Difference Location of the Ludian  $M_s$ 6.5 Earthquake Sequences in Yunnan Province in 2014. *Chinese Journal of Geophysics*, 57(9): 3042–3051 (in Chinese with English Abstract)
- Wen, X. Z., Du, F., Yi, G. X., et al., 2013. Earthquake Potential of the Zhaotong and Lianfeng Fault Zones of the Eastern Sichuan-Yunnan Border Region. *Chinese Journal of Geophysics*, 56(10): 3361–3372 (in Chinese with English Abstract)
- Wen, X. Z., Ma, S. L., Xu, X. W., et al., 2008. Historical Pattern and Behavior of Earthquake Ruptures along the Eastern Boundary of the Sichuan-Yunnan Faulted-Block, Southwestern China. *Physics of the Earth and Planetary Interiors*, 168(1/2): 16–36. <https://doi.org/10.1016/j.pepi.2008.04.013>
- Wieczorek, G. F., 1984. Preparing a Detailed Landslide-Inventory Map for Hazard Evaluation and Reduction. *Environmental & Engineering Geoscience*, XXI(3): 337–342. <https://doi.org/10.2113/gsegeosci.xxi.3.337>
- Wu, C. H., Cui, P., Li, Y. S., et al., 2018. Seismogenic Fault and Topography Control on the Spatial Patterns of Landslides Triggered by the 2017 Jiuzhaigou Earthquake. *Journal of Mountain Science*, 15(4): 793–807. <https://doi.org/10.1007/s11629-017-4761-9>
- Xie, Z. J., Zheng, Y., Liu, C. L., et al., 2015. Source Parameters of the 2014  $M_s$ 6.5 Ludian Earthquake Sequence and Their Implications on the Seismogenic Structure. *Seismological Research Letters*, 86(6): 1614–1621. <https://doi.org/10.1785/0220150085>
- Xu, C., 2015a. Preparation of Earthquake-Triggered Landslide Inventory Maps Using Remote Sensing and GIS Technologies: Principles and Case Studies. *Geoscience Frontiers*, 6(6): 825–836. <https://doi.org/10.1016/j.gsf.2014.03.004>
- Xu, C., 2015b. Utilizing Coseismic Landslides to Analyze the Source and Rupturing Process of the 2014 Ludian Earthquake. *Journal of Engineering Geology*, 23(4): 755–759 (in Chinese with English Abstract)

- Xu, C., Xu, X. W., 2014. The Spatial Distribution Pattern of Landslides Triggered by the 20 April 2013 Lushan Earthquake of China and Its Implication to Identification of the Seismogenic Fault. *Chinese Science Bulletin*, 59(13): 1416–1424. <https://doi.org/10.1007/s11434-014-0202-0>
- Xu, C., Xu, X. W., Yao, X., et al., 2014a. Three (Nearly) Complete Inventories of Landslides Triggered by the May 12, 2008 Wenchuan  $M_w7.9$  Earthquake of China and Their Spatial Distribution Statistical Analysis. *Landslides*, 11(3): 441–461. <https://doi.org/10.1007/s10346-013-0404-6>
- Xu, C., Xu, X. W., Shen L. L., 2014b. Inventory of Landslides Triggered by the 2014  $M_s6.5$  Ludian Earthquake and Its Implications on Several Earthquake Parameters. *Seismology and Geology*, 36(4):1186–1203 (in Chinese with English Abstract)
- Xu, C., Xu, X. W., Tian, Y. Y., et al., 2016. Two Comparable Earthquakes Produced Greatly Different Coseismic Landslides: The 2015 Gorkha, Nepal and 2008 Wenchuan, China Events. *Journal of Earth Science*, 27(6): 1008–1015. <https://doi.org/10.1007/s12583-016-0684-6>
- Xu, J. X., Xu, C., He, X. L., et al., 2020. Spatial Distribution of Seismic Landslides in the Areas of 1927 Gulang  $M8.0$  Earthquake. *Earthquake Research in China*, 34(1): 5–28 (in Chinese with English Abstract)
- Xu, L. S., Zhang, X., Yan, C., et al., 2014. Analysis of the Love Waves for the Source Complexity of the Ludian  $M(s)6.5$  Earthquake. *Chinese Journal of Geophysics*, 57(9): 3006–3017 (in Chinese with English Abstract)
- Xu, X. W., Jiang, G. Y., Yu, G. H., et al., 2014. Discussion on Seismogenic Fault of the Ludian  $M_s6.5$  Earthquake and Its Tectonic Attribution. *Chinese Journal of Geophysics*, 57(9): 3060–3068 (in Chinese with English Abstract)
- Xu, X. W., Wen, X. Z., Zheng, R. Z., et al., 2003. Pattern of Latest Tectonic Motion and Its Dynamics for Active Blocks in Sichuan-Yunnan Region, China. *Science in China Series D: Earth Sciences*, 46(2): 210–226. <https://doi.org/10.1360/03dz0017>
- Xu, X. W., Xu, C., 2021. Natural Hazards Research: An Eternal Subject of Human Survival and Development. *Natural Hazards Research*, 1(1): 1–3. <https://doi.org/10.1016/j.nhres.2020.12.003>
- Xu, X. W., Xu, C., Yu, G. H., et al., 2015. Primary Surface Ruptures of the Ludian  $M_w6.2$  Earthquake, Southeastern Tibetan Plateau, China. *Seismological Research Letters*, 86(6): 1622–1635. <https://doi.org/10.1785/0220150038>
- Zhang, G. W., Lei, J. S., Liang, S. S., et al., 2014. Relocations and Focal Mechanism Solutions of the 3 August 2014 Ludian, Yunnan  $M_s6.5$  Earthquake Sequence. *Chinese Journal of Geophysics*, 57(9): 3018–3027 (in Chinese with English Abstract)
- Zhang, P. Z., Deng, Q. D., Zhang, G. M., et al., 2003. Active Tectonic Blocks and Strong Earthquakes in the Continent of China. *Science in China Series D: Earth Sciences*, 46(2): 13–24. <https://doi.org/10.1360/03dz0002>
- Zhang, S. C., Wang, S. J., Diao, G. L., et al., 1994. The Rupture Characteristics of 1974 Yongshan-Daguan Earthquake Sequence. *Acta Geophysica Sinica*, 170–176 (in Chinese with English Abstract)
- Zhang, Y., Xu, L. S., Chen, Y. T., et al., 2014. Rupture Process of the 3 August 2014 Ludian, Yunnan,  $M_w6.1$  ( $M_s6.5$ ) Earthquake. *Chinese Journal of Geophysics*, 57(9): 3052–3059 (in Chinese with English Abstract)
- Zhao, K., Lin, G. L., Yang, L., et al., 2020. Strong Motion Record Analysis of the Qiaojia  $M_s5.0$  Earthquake in Yunnan Province. *Seismological and Geomagnetic Observation and Research*, 41(3): 200–208 (in Chinese with English Abstract)
- Zhu, C. N., Chen, C. Z., 1976. The Rupture Mechanism of the Zhaotong Earthquake of 1974 in Yunnan Province. *Chinese Journal of Sinica*, 19(4): 317–329 (in Chinese with English Abstract)